Front. Environ. Sci. Eng. 2020, 14(2): 23
https://doi.org/10.1007/s11783-019-1202-8

REVIEW ARTICLE

$PM_{2.5}$ over North China based on MODIS AOD and effect of meteorological elements during 2003–2015

Youfang Chen[1,2], Yimin Zhou[1,2], Xinyi Zhao (✉)[1,2]

1 College of Urban and Environmental Sciences, Peking University, Beijing 100871, China
2 Key Laboratory for Earth Surface Processes of the Ministry of Education, Peking University, Beijing 100871, China

HIGHLIGHTS

- The Taihang Mountains was the boundary between high and low pollution areas.
- There were one high value center for $PM_{2.5}$ pollution and two low value centers.
- In 2004, 2009 and after 2013, $PM_{2.5}$ concentration was relatively low.

GRAPHIC ABSTRACT

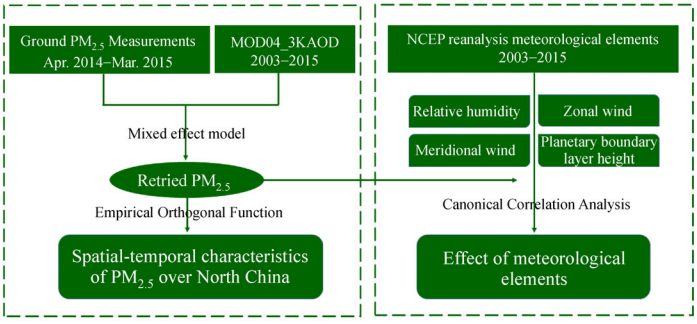

ARTICLE INFO

Article history:
Received 10 January 2019
Revised 18 October 2019
Accepted 4 November 2019
Available online 16 December 2019

Keywords:
Aerosol optical depth
$PM_{2.5}$
MODIS
Mixed effect model
Canonical correlation analysis

ABSTRACT

Over the past 40 years, $PM_{2.5}$ pollution in North China has become increasingly serious and progressively exposes the densely populated areas to pollutants. However, due to limited ground data, it is challenging to estimate accurate $PM_{2.5}$ exposure levels, further making it unfavorable for the prediction and prevention of $PM_{2.5}$ pollutions. This paper therefore uses the mixed effect model to estimate daily $PM_{2.5}$ concentrations of North China between 2003 and 2015 with ground observation data and MODIS AOD satellite data. The tempo-spatial characteristics of $PM_{2.5}$ and the influence of meteorological elements on $PM_{2.5}$ is discussed with EOF and canonical correlation analysis respectively. Results show that overall R^2 is 0.36 and the root mean squared predicted error was 30.1 $\mu g/m^3$ for the model prediction. Our time series analysis showed that, the Taihang Mountains acted as a boundary between the high and low pollution areas in North China; while the northern part of Henan Province, the southern part of Hebei Province and the western part of Shandong Province were the most polluted areas. Although, in 2004, 2009 and dates after 2013, $PM_{2.5}$ concentrations were relatively low. Meteorological/topography conditions, that include high surface humidity of area in the range of 34°–40°N and 119°–124°E, relatively low boundary layer heights, and southerly and easterly winds from the east and north area were common factors attributed to haze in the most polluted area. Overall, the spatial distribution of increasingly concentrated $PM_{2.5}$ pollution in North China are consistent with the local emission level, unfavorable meteorological conditions and topographic changes.

1 Introduction

Air pollution caused by fine particulate matter (aerodynamic diameters of less than 2.5 μm, $PM_{2.5}$) has become a major environmental challenge in the 21st century. Increasing research has shown that aerosols have large influences on clouds and precipitation (Koren et al., 2012; Wang et al., 2016; Guo et al., 2016; Jiang et al., 2018), climate system (Kaufman et al., 2002) and public health (Gu and Yim, 2016). With rapid industrial development, extensive transportation networks and extremely dense population, North China has one of the highest concentrations of atmospheric aerosols in the world (Remer et al., 2005; Levy et al., 2010; Guo et al., 2014) with the number of hazy days significantly increased since the 1980s (Fan and Chun, 2008; Hu and Zhou, 2009; Wu et al., 2010). What's more, prolonged heavy pollution episodes occur

✉ Corresponding author
E-mail: sh-zhao@urban.pku.edu.cn

more and more frequently. According to the 2013 annual air quality data of 74 major cities issued by the Ministry of Environmental Protection (MEP) of China, the annual average $PM_{2.5}$ concentrations in all cities in the Beijing-Tianjin-Hebei region exceeded the standard, among which 7 cities ranked in the top 10. The number of days of pollution for some cities accounted for 40% of the total number of days of the year. Taking Beijing as an example, Beijing has experienced rapid expansions in economy and urbanization over the past several decades. From 2009 to 2013, the gross domestic product (GDP) in Beijing increased from $203 to $325 billion, however, vehicle numbers in the city have increased from 4.0 to 5.4 million – contributing to a steady deterioration in air quality since the 1990s. Pollution levels are further highlighted with average annual $PM_{2.5}$ concentrations in 2013 reaching 102 $\mu g/m^3$, with the daily maximum $PM_{2.5}$ value reaching 568 $\mu g/m^3$ (Zhang et al., 2013; Guo et al., 2014; Sun et al., 2014; Zhang et al., 2015; Zhang and Cao, 2015).

The adverse effects of polluted weather therefore creates an urgent demand on obtaining daily high resolution $PM_{2.5}$ concentration data and its spatio-temporal variations – allowing more effective means of predicting and enacting $PM_{2.5}$ pollutions control. Currently, ground-based observations provide precise and timely concentration of atmospheric $PM_{2.5}$. However, due to limited spatial and temporal coverage, in situ observations are unable to capture high resolution tempo-spatial $PM_{2.5}$ concentration variation – this is particular for many developing countries such as China, because of high operational cost and technology requirements (Wang et al., 2017). As such satellite remote sensing can provide aerosol optical depth (AOD) products at various scales to assist retrieve $PM_{2.5}$ air quality for areas where surface ground-based $PM_{2.5}$ monitors are not available or too sparse (Liu et al., 2004; Engel-Cox et al., 2006; Gupta and Christopher, 2008; van Donkelaar et al., 2011;Zhang et al., 2017a). AOD data are composed of non-dimensional parameters calculated by integrating light extinction of aerosols from the ground-level with the top of the atmosphere and its reflection of the integrated particles in a vertical column – this represents PM loading in the air (Dinoi et al., 2010; Hu et al., 2014; Ghotbi et al., 2016). Among many satellite AOD products, the Moderate Resolution Imaging Spectroradiometer (MODIS) AOD is most widely used to retrieved $PM_{2.5}$ due to its high resolution and accuracy (Liu et al., 2005; van Donkelaar et al., 2011). Wang and Christopher (2003) initially used MODIS AOD in the prediction of ground level $PM_{2.5}$ in the USA in 2003 and numerous researchers have attempted to estimate ground $PM_{2.5}$ level after that.

The retrieved methods mainly included simple linear model, land use regression model, geographically weighted regression, and complex model with additional variables (Wang and Christopher, 2003; Liu et al., 2009; Kloog et al., 2012; Hu et al., 2014; Ma et al., 2014; Bai et al., 2016). The relationship between $PM_{2.5}$ and AOD in these methods is fixed, though the inversion effects of these methods can vary. Particle size, composition and the vertical profile of aerosols in atmospheric column or other PM properties could however affect the optical properties of particles, due to the spatio-temporal change of local emissions, meteorological elements or other impact factors. Consequently, it is understood that the $PM_{2.5}$-AOD relationship changes as the spatio-temporal paramters change (Liu et al., 2007; Lee et al., 2011). That's to say, the relationship between $PM_{2.5}$ and AOD varies by day. Therefore, in this paper we considered the daily variability and location difference in the retrieval and later prediction of $PM_{2.5}$ ground concentration data via MODIS AOD.

Mixed models are adopted as they are statistical models containing both fixed effects and random effects. These models are particularly useful in situations where repeated measurements are made on the same statistical units, or where measurements are made on clusters of related statistical units. In the 1950s, Henderson provided best linear unbiased estimates (BLUE) of fixed effects and best linear unbiased predictions (BLUP) of random effects (Henderson, 1948). From then on, mixed modeling has become a major area of statistical research. Lee et al. (Lee et al., 2011) introduced this method to $PM_{2.5}$ by developing a linear mixed effects (LME) model with day-specific random effects for AOD, which can account for daily variations of $PM_{2.5}$-AOD relationship. Previous studies have shown that day-specific LME model performs better than other statistical models such as (GWR) (Ma et al., 2016) and linear regression model (Lee et al., 2011). Due to its high accuracy, the day-specific LME model has been widely applied in many studies and models worked well in different areas (Kloog et al., 2012; Hu et al., 2014; Beloconi et al., 2016; Lee et al., 2016). However, the LME model has not been widely used in retriving $PM_{2.5}$ concentrations in China. Specifically, no long-term sequence studies on highly polluted areas in China have been found, the likes of which are essential to the assessment and prevention of $PM_{2.5}$ pollution.

As mentioned before, the increase of emissions with rapid urbanization and economic development are generally considered as the primary reason for the increase of polluted days in China. However, the observed air pollution has significant interannual and decadal variability (Guo et al., 2011; Chen et al., 2019) in contrary to the persistent and rapid increase of total local energy consumption (Li et al., 2016; Wang et al., 2016) – these variabilities are recognized to be associated with the changes in climate models. Consequently, in addition to analyzing spatio-temporal variations of $PM_{2.5}$ over North China based on remote sensing AOD data, we further explore the effect of meteorological elements on $PM_{2.5}$ concentrations.

2 Data and methods

2.1 Study area

Our study area of North China includes all areas of Beijing, Tianjin, Hebei, Shandong and parts of Shanxi, Henan, Inner Mongolia and Liaoning (Fig. 1) – where latitude and longitude ranges are from 34°N to 43°N, 113°E to 123°E. In northern China, most areas are warm temperate semi-monsoon climate, and a small part of the north-west sits within the Loess Plateau region. Due to the Taihang Mountains, the altitude in the study area is higher in the west and lower in the east, with an average altitude of about 50 m.

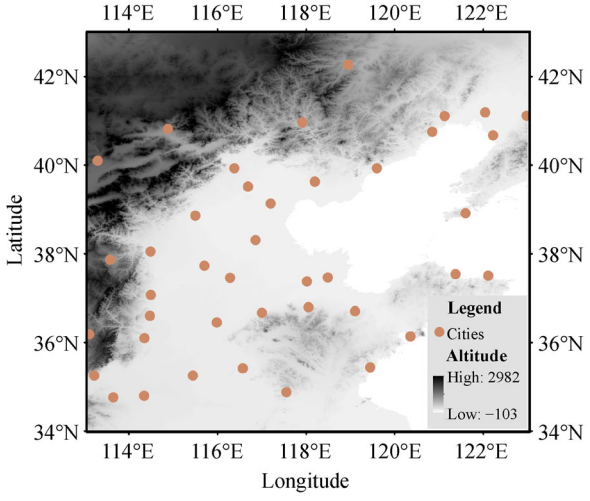

Fig. 1 Study area location and spatial distribution of cities involved with $PM_{2.5}$ monitoring sites in this study. In total there are 215 monitoring sites in 41 cities. Red points represent the cities, where altitude is represented by the gray color bar.

2.2 Data

2.2.1 Ground $PM_{2.5}$ measurements

Hourly $PM_{2.5}$ measurements from Apr. 2014 to Mar. 2015 were collected from the official MEP of China website (http://air.epmap.org/). The MEP has released $PM_{2.5}$ data in major cities since 2013. According to the Chinese National Ambient Air Quality Standard (CNAAQS, GB3095-2012, available on the MEP website http://kjs.mep.gov.cn/), the ground $PM_{2.5}$ data of China are measured by the tapered element oscillating microbalance method (TEOM) or the beta-attenuation method. A total of 215 monitoring sites that meet the requirements of Technical Regulation for Selection of Ambient Air Quality Monitoring Stations (on trial) (HJ 664-2013) in 41 cities are included within our study area (Fig. 1). In this study, hourly $PM_{2.5}$ data was recorded between 11:00 and 15:00 (local time) at the ground stations. Data was averaged to match the AOD retrieval time of 13:30. $PM_{2.5}$ pollution days are defined as days with an average $PM_{2.5}$ concentration over 75 $\mu g/m^3$ – as based on CNAAQS. A pollution day ratio was defined by dividing days with $PM_{2.5}$ concentration data by the days with $PM_{2.5}$ concentrations larger than 75 $\mu g/m^3$. This was to create a standard to measure/account for degrees of contamination of an observation area or observation point due to missing satellite data.

2.2.2 MODIS 3 km AOD Product

The MODIS aerosol level 2 products during 2003–2015 over study area were acquired from the Level 1 Atmosphere Archive and Distribution System (LAADS) (Levy & Hsu, 2015). MODIS carried on the NASA Terra satellite was launched in May 2002 and has been providing retrieval products of aerosol properties with nearly daily global coverage since 2003. The satellite crosses our study region at approximately (on average) 13:30 local time with a scanning swath of 2330 km (cross-track) by 10 km (along-track at nadir). Using dark target algorithms, the MODIS AOD over land is retrieved using the spectral information at three channels of 0.47, 0.66 and 2.12 m (Remer et al., 2005) to acquire average signals of atmospheric aerosols in the vertical direction. The uncertainty of the MODIS AOD measurements is expected to be $1AOD = 0.05 \pm 0.15 \times AOD$ over land (Levy et al., 2010). Standard MODIS Level 2 (L2) AOD products are distributed at a 10 km resolution. In early 2014, NASA released the new collection 6 (C006) AOD products at a 3 km resolution (MYD04_3K) making it possible for air quality observers to estimate $PM_{2.5}$ with a higher resolution. The retrieval algorithm of the higher resolution product is similar to that of the 10 km standard product but averages 6×6 pixels in a single retrieval box rather than the 20×20 pixels after cloud screening and other surface mask processes (Levy et al., 2013; Munchak et al., 2013). The resolution of grid cells was determined to be 3 km × 3 km under the Mercator projection. There were 76 grid cells in the x direction and 100 cells in the y direction (7600 cells in total) in our study area.

2.2.3 NCEP reanalysis meteorological data

Meteorological parameters can impact optical properties of particles by affecting chemical composition or physical properties of particles directly or indirectly, which further influence the formation and transport of $PM_{2.5}$ (Sotoudeheian and Arhami, 2014; Ghotbi et al., 2016). Consequently, we also explored the effect of meteorological elements on $PM_{2.5}$ in addition to analyzing its spatio-temporal characteristics. The meteorological data used in our study included: relative humidity (RH), wind speed

(Uwind and Vwind) and planetary boundary layer height (PBLH) during 2003–2015. Meteorological data was obtained from the National Centers Environmental Prediction (NCEP) and National Center for Atmospheric Research (NCAR). Data during January 2003 and June 2007 was extracted from NCAR/NCEP reanalysis (R1) and between July 2007 and December 2015 from NCEP/DOE Reanalysis 2 (R2). Through four-dimensional assimilation analysis, various observations and model output data are produced into high-quality global meteorological data sets, referred to as NCAR/NCEP reanalysis data. The time resolution of the data was set at 6 h intervals, which were at Beijing time 08:00, 14:00, 20:00, and 02:00 the next day, with a spatial resolution of 1° × 1° (http://rda.ucar.edu/datasets/ Ds083.2). Since meteorological elements in the boundary layer do not have large-scale and long-term observation results, the reanalysis of meteorological data are commonly used in atmospheric sciences as actual historical data. The reanalyzed data, as long-term meteorological data, is currently considered to be the closest to actual historical data and widely used in atmospheric scientific research, especially in climate simulation and climate diagnosis (Trenberth et al., 2014; Wang and Chen, 2014). Numerous studies have compared reanalysis data and observation data to prove its reliability (Kalnay et al., 1996; Zhao et al., 2004). We chose the data at 14:00 to match the satellite observed time. Since the spatial resolution of the meteorological elements differs significantly from $PM_{2.5}$, the $PM_{2.5}$ concentration data was resampled to the same 1° × 1° as the reanalysis data resolution when analyzing the relationship between them. The data used was summarized as Table 1.

2.3 Methods

2.3.1 Mixed effect model

This paper makes use of the ground observation data of 41 cities and MODIS AOD data during Apr. 2014 – Mar. 2015 to construct a relation model of $PM_{2.5}$ and AOD in North China through the Mixed effect model (Lee et al., 2011; Xie et al., 2015), and then obtains long-terrm daily $PM_{2.5}$ concetration bewteen 2003 and 2015 via the AOD product.

We calibrated AOD data of MYD04 using the ground-based $PM_{2.5}$ concentration data first. Hourly ground $PM_{2.5}$ concentration data of 41 cities was used to take the average value from 11:00 to 15:00 as the city's daily value for calibration to match the satellite crossing time. AOD data takes the average of the AOD values of all grids within each city range on the day as the daliy value of the city. In this way, daily $PM_{2.5}$ concentration data and corresponding AOD data for each city during April to December 2014 can be obtained to retrieve the parameters in the mixed effect model (Eq. (1)).

$$PM_{2.5ij} = (\alpha_{\text{fixed}} + \alpha_j) + (\beta_{\text{fixed}} + \beta_j) \times AOD_{ij} + s_i + \varepsilon_{ij}(\alpha_j\beta_j) \sim N_{[(00),\Sigma]} \quad (1)$$

Where $PM_{2.5ij}$ and AOD_{ij} are their value at city i on day j. Where α_{fixed} and β_{fixed} are the fixed intercept and slope respectively, and α_j and β_j are the random intercept and slope. S_i is the random intercept of site i, ε_{ij} is the error term at site i on day j and Σ is the variance-covariance matrix for the day-specific random effects. The random parameters can represent the temporal and spatial variation of AOD-$PM_{2.5}$ relationships, which help to retrieved more accurate daily $PM_{2.5}$ concentrations. We chose MODIS AOD data to match the $PM_{2.5}$ data of 41 cities in the study area from April 2014 to December 2014 and used these pairs of data to create the mixed effect model.

2.3.2 EOF analysis

Taking into account missing data and outlier values, we calculated average $PM_{2.5}$ concentration during every quarter as quarterly data. Average daily value in the first two months in 2003 and last two months in 2015 were both calculated as a quarterly value respectively. Consequently, we had 53 quarters which were then analyzed via temporal and spatial characteristics using the quarterly pollution day ratio data by Empirical Orthogonal Function (EOF). EOF, also known as Eigenvector Analysis, or Principal Component Analysis (PCA), is an analysis of structural features by a few principal components in matrix data. (Lorenz, 1956) introduced it to meteorology and climate research for the first time in the 1950s and is now widely used in geosciences and hydroacoustics. EOF analysis is capable of decomposing the time-varying signal or data set into a part of the spatial function and a time function part. The spatial function part does not change with time and can summarize the geographical distribution characteristics of the data, and the time function part which only depends on the time variation is composed of a linear combination of variables and thus can show time changes in data. The first few decomposed components occupy a large part of the total variance of original siginals, which can been seen as

Table 1 Data introduction

Parameters	Time range	Data sources	Resolution
MODIS AOD	2003–2015	MYD04_3 km data set	Daily, 3 km × 3 km
$PM_{2.5}$ measurements	Apr. 2014 – Mar. 2015	MEP of PRC	Hourly, cities
Meteorological elements	2003–2015	NCAR/NCEP reanalysis (R1), NCEP/DOE Reanalysis 2 (R2)	Every 6 h, 1° × 1°

that the main information of original siginals are concentrated on these components. This method is quick to converge and it is easy to concentrate a large amount of data. It can decompose irregularly distributed sites within a limited area, and the decomposed spatial structure has a clear physical meaning. That's to say, it can find both time series and spatial patterns of $PM_{2.5}$.

2.3.3 Canonical correlation analysis

Canonical correlation analysis (CCA), first proposed by Hotelling (1936), is a multivariate statistical method that uses the correlation between comprehensive variables to reflect the overall correlation between the two sets of variables. We used it to analyze the relationship between $PM_{2.5}$ and meteorological elements. Like EOF analysis, CCA analysis extracts typical variables formed by representative number of representative variables from original variables. However, the variables here are two groups of data sets, in order to make the correlation between the two groups of indicators clear. The correlation between these comprehensive variables represented by typical correlation coefficient is used to reflect the overall correlation between the two groups of data sets – when the typical correlation coefficient is less than 0.3 the corresponding feature vectors are generally not significant.

Under the resolution of meteorological data, the study area was divided into 10 × 11 total 110 grid points. Though CCA does not require uniform data resolution for the two variable fields, we selected days where there are $PM_{2.5}$ data in half of the grids. We then resampled the $PM_{2.5}$ data to the same resolution as the meteorological data to mitigate missing data effects. A total of 2145 days were selected for the CCA analysis.

2.4 Mixed effects mode validation

To assess the fitting performance of the model inversion, coefficient of determination (R^2), mean prediction error (MPE), and root mean squared prediction error (RMSE) between model estimations and ground observations were calculated.

R^2 of most cities passed the credibility test of 0.01 credibility test ($P < 0.01$), Weihai, Qingdao, and Texas passed the credibility test of 0.1 ($P < 0.1$) and Qinhuangdao, Heze, Datong and Huludao passed the 0.05 confidence test ($P < 0.5$), but Zaozhuang and Zhengzhou failed to pass the 0.1 credibility test ($P > 0.1$). Consequently, we used the data of the 39 cities that passed a reliability of 0.1 to build the mixed effect model in the following discuss. In general, the correlation coefficient of northern cities was slightly higher than that of southern cities, especially the correlation coefficient for the cities between southern Hebei, northern Henan, and southern Shandong. These cities are usually heavily polluted areas of $PM_{2.5}$. That is to say, model fitting results were poorer for areas with severe $PM_{2.5}$ pollution, while results were better in less polluted areas.

A total of 1973 pairs of data points dated from between April to December 2014 of 36 cities that passed 0.01 confidence were selected to test the model. R^2 for retrived $PM_{2.5}$ and observed $PM_{2.5}$ was increased above the AOD and observed $PM_{2.5}$. MPE and RMSE were 21.6 and 30.1, respectively (Fig. 2). To test the stability of the model parameters, we also verified 141 pairs of data in 8 cities in 2015 and 885 pairs of data in 12 cities in 2017. The MPE were 25.6 and 20.97 and RMSE were 38.5 μg/m^3 and 22.21 μg/m^3 for 2015 and 2017, respecticely, which indicated the relationship between data and the ground $PM_{2.5}$ from MEP of PRC and MODIS AOD we developed was relatively robust.

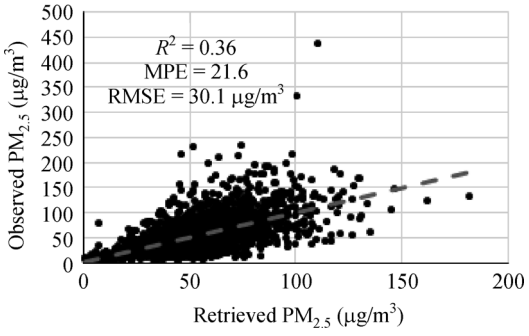

Fig. 2 Plots of fitting performance of retrieved $PM_{2.5}$ and observed $PM_{2.5}$ during Apr. – Dec. 2014. The gray line denotes the fitted linear regression line.

3 Results and discussion

3.1 Spatial and temporal variability in $PM_{2.5}$ levels

EOF analysis of quarterly anomalies of the pollution day ratio over North China was used to examine the spatial and temporal variability in $PM_{2.5}$ levels. According to the EOF decomposition, the variance contribution rate of the first spatial modality was about 80% (the first spatial modality captured about 80% signal of the $PM_{2.5}$ spatial distribution characteristics). Therefore, the first modality map represented the spatial distribution of $PM_{2.5}$ concentrations in North China from 2003 to 2015 largely. To further understand the actual spatial distribution of the $PM_{2.5}$ concentrations, we calculated the average concentration of all days in each grid with retrieved $PM_{2.5}$ data. From 2003 to 2015, the spatial distribution of the average $PM_{2.5}$ concentrations were effectively the same with the first mode of the EOF decomposition, presenting the distribution characteristics of two low-value areas and one high-value area. $PM_{2.5}$ concentration in the high-value center was around 70 μg/cm^3, and the low value center was below 20 ug/cm^3 (Fig. 3). The Taihang Mountains were the

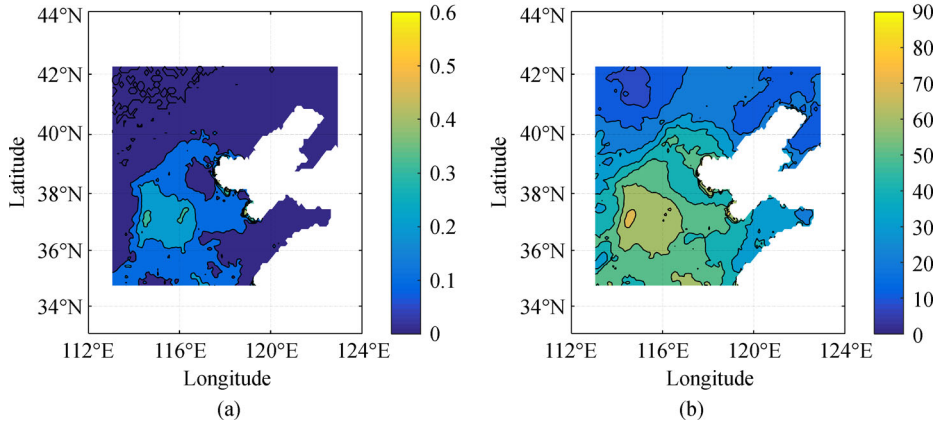

Fig. 3 (a) Conventional first mode of EOF (EOF1) of $PM_{2.5}$ over North China based on quarterly pollution day ratio for the period of 2003–2015. Percentages of explained variance are printed at the upper left on the EOF maps. (b) Daily mean $PM_{2.5}$ concentrations during 2003−2015, the unit for the legend is μg/cm^3.

obvious dividing line with lower pollution in the north-west region and higher $PM_{2.5}$ concentrations in the south-eastern areas. That's to say, pollution in the southern part of the study area was significantly higher than that in the north and the Shandong Peninsula, among which the southern part of Hebei Province, northern part of Henan Province and the western part of Shandong Province were the most polluted areas (core pollution areas). The number of pollution days in the core pollution areas were about 5 times the average value of the entire study area (Fig. 4(a)). The degree of pollution in the surrounding areas were second only to this area, and the pollution levels in the north and south areas are slightly higher than those in the east and west areas. Previous studies have also confirmed the impact of mountains between cities on $PM_{2.5}$ concentrations (Wang et al., 2017). The dividing line is also consistent with the low-to-high demarcation line and the humid and semi-humid areas transition line.

This spatial distribution feature was also consistent with the results of many other different spatial scale studies (Ma et al., 2014; Lv et al., 2017; Wei et al., 2017). There are two main reasons for this. On the one hand, the plain area was the main industrial production area – particularly substantially polluting heavy industry. Take Hebei, a severe pollution area, as an example, heavy industry accounted for more than 65% in 2015 on the total profit of the above-scale enterprises (enterprise above designated size). On the other hand, due to the obstruction of the mountain and different climate on each side of the mountains, the pollution generated in the plain area could not be spread to the north-western region.

As for the temporal distribution, $PM_{2.5}$ concentration had obvious annual and interannual trends. There were 13 morphologically distinct peaks in PC1, which demonstrated the annual change of $PM_{2.5}$ concentrations. More generally, $PM_{2.5}$ concentrations over North China experienced three distinct declines according to PC1 (Fig. 4(a)). Pollution in 2003 was heavy, while declined sharply in 2004. This was also confirmed by other research results though $PM_{2.5}$ or AOD retrieved using different data and methods in those papers (Sun and Chen, 2017; Zhang et al., 2017b). Because of lack of earlier data and no

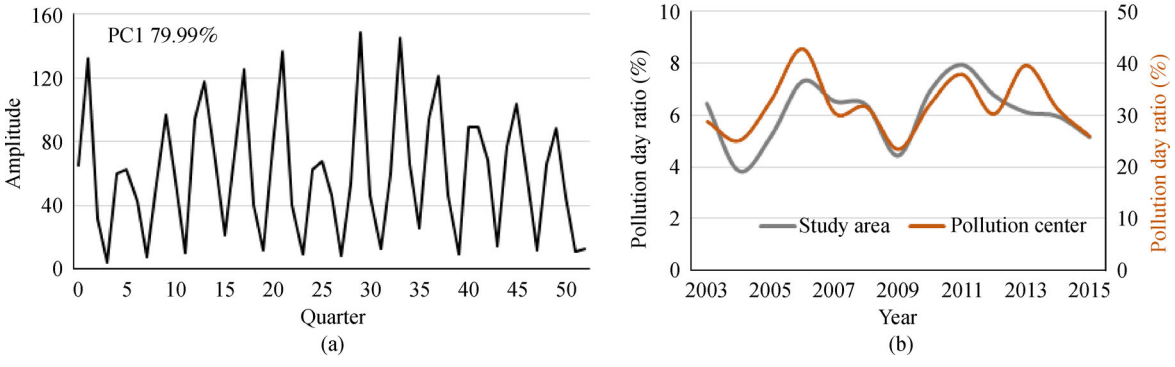

Fig. 4 (a) Conventional first principal component (PC1) of $PM_{2.5}$ over North China based on quarterly pollution day ratio for the period of 2003–2015. Percentages of explained variance are printed at the upper left on the PC maps. (b) Pollution day ratio during study period, red line represented the pollution day ratio of the pollution core areas and gray line indicated across the study area.

articles have been found to discuss this issue, it is difficult to figure out $PM_{2.5}$ concentrations before 2003, consequently we couldn't deduce the possible reason for the high value of 2003 or the very low value of 2004. $PM_{2.5}$ pollution continued to increase (a high value interval) in the next period of 2004 to 2008 but dropped down drastically in 2009 where the second low $PM_{2.5}$ pollution point appeared. To ensure the smooth convening of the Beijing 2008 Olympic Games, the Chinese government has implemented many measures to reduce emissions and production, which was bound to be one of the reasons that contributed to the low $PM_{2.5}$ concentrations between 2008 and 2009. However, $PM_{2.5}$ pollution has risen sharply again after 2009 with a peak value in 2013 during this period. Fortunately, it showed a trend of gentle fluctuations since 2013 until the end of the retrieved data we currently have. Research by Zheng et al. also confirmed this trend, further showing that annual mean $PM_{2.5}$ concentrations decreased by 21.5% over China during 2013–2015 (Zheng et al., 2017). This interannual fluctuation can be similarly obtained by calculating the annual pollution day ratio of the polluted core area and the whole study area using the retrieved data (Fig. 4(b)).

3.2 Relationship between meteorological elements and $PM_{2.5}$

Severe atmospheric pollution is closely related to: high emission intensity and emission sources, unfavorable meteorological conditions, special terrain, pollutant transport and chemical conversion in the atmosphere. As such, the degree of pollution in an area depends on the area's energy structure, traffic conditions and the number of industrial pollutants emitted from a long-term or average point of view (Zhang et al., 2009; Chen et al., 2009; Cao et al., 2011; Pearce et al., 2011). However, in terms of short-term or real-time status, it is mainly related to the local weather conditions at that time. Large-scale circulation patterns and local meteorological conditions cannot only affect the generation, accumulation, and removal of pollutants by affecting chemical composition or physical properties of particles directly or indirectly, but can also act as important external conditions that affect regional transportation (Fang et al., 2007; Ghotbi et al., 2016). For example, Tai et al. found that daily variation in meteorology can explain up to 50% of $PM_{2.5}$ variability as described by the multiple linear regression model (Tai et al., 2010). To explore these effects on $PM_{2.5}$, meteorological parameters (including RH, Uwind, Vwind and PBLH) were considered on our CCA analysis. What's more, meteorological elements have vertical structure and the elements of each pressure layer on the vertical height varies, so the impact on $PM_{2.5}$ may also be different. Consequently, this paper also analyzed the relationship between meteorological elements and $PM_{2.5}$ on different pressure levels at vertical height. Results can be found in Table 2.

The canonical correlation coefficient (CCC) between $PM_{2.5}$ and meteorological elements decreased as the air pressure decreased in the vertical profile. Which means $PM_{2.5}$ concentrations were mainly impacted by meteorological elements of the ground and bottom atmosphere. Consequently, we used ground meteorological data to analyze its relationship with $PM_{2.5}$. The first typical factor of all meteorological elements is seen as factors influencing high-value pollution centers, which confirmed the spatial characteristics above again.

3.2.1 RH & $PM_{2.5}$

Relative humidity can affect particle formation rate through photochemical oxidation and a condensation process, imposing different particle compositions (Ghotbi et al., 2016). Simialry, variation of relative humidity has influence on size distribution and optical physiochemical properties of aerosols through hygroscopic particles growth or photochemistry phenomena (Marcazzan et al., 2001). Therefore, we divided the relative humidity from 0 to 100% into 4 intervals and calculated the $PM_{2.5}$ concentrations at the corresponding time in each relative humidity interval. Figure 5 shows the percentage of pollution day ratio in the entire study area under different relative humidity intervals. From the results we can see that $PM_{2.5}$ pollution intensity and relative humidity showed a clear positive correlation; the higher the relative humidity, the stronger the pollution level. As relative humidity increases, the more aerosol particles in the air, the better the formation and development of fine particulate matter. Especially in the polluted core area (yellow area), where the pollution level was significantly higher than that of other areas at the same relative humidity – with the degree of pollution declining outwardly in the form of concentric rings.

Based on the correlation coefficient of typical variables, we can know that $PM_{2.5}$ concentration in the south-western extension of the North China region was positively related to the relative humidity in the range of 34°–40°N and 119°–124°E. In the eastern region, $PM_{2.5}$ pollution was mainly negatively correlated with the relative humidity of 34°–39°N and 112°–120°E, whereas the concentration of $PM_{2.5}$ in the north-western region was mainly influenced by the relative humidity in the central and north regions (Fig. 6). Relationship between RH and $PM_{2.5}$ saw little change until the pressure layer was around 850mb. Meteorological conditions at 850mb can reflect the regional circulation – where circulation tends to be simple above this value. Therefore, the control range of major meteorological factors is larger and tends to be simpler. That is to say, the control ability strengthens, which can also be seen from the fact that the correlation coefficient at 850mb height was inconsistent with the trend of rising and falling height. We know that the Taihang Mountains is an

Table 2 Canonical correlation coefficient (CCC) between $PM_{2.5}$ concentration and meteorological elements at different vertical height

Meteorological elements	Pressure layer(hPa)	First CCC	Second CCC	Third CCC	Fourth CCC	Fifth CCC	Sixth CCC
RH[a)]	Surface	0.64	0.51	0.46	0.45	0.44	0.43
	1000	0.67	0.52	0.46	0.44	0.43	0.42
	975	0.65	0.52	0.47	0.44	0.44	0.42
	950	0.64	0.50	0.46	0.44	0.42	0.42
	925	0.63	0.48	0.44	0.43	0.41	0.41
	900	0.63	0.47	0.43	0.42	0.41	0.40
	850	0.64	0.45	0.42	0.41	0.41	0.40
	800	0.60	0.46	0.42	0.41	0.41	0.40
	750	0.57	0.47	0.43	0.43	0.42	0.41
	700	0.54	0.45	0.43	0.43	0.42	0.41
Uwind[b)]	Surface	0.63	0.50	0.44	0.44	0.43	0.42
	1000	0.59	0.47	0.45	0.44	0.43	0.42
	975	0.59	0.47	0.45	0.44	0.44	0.43
	950	0.58	0.47	0.44	0.44	0.43	0.43
	925	0.57	0.47	0.44	0.44	0.43	0.43
	900	0.56	0.47	0.44	0.44	0.44	0.43
	850	0.56	0.46	0.44	0.44	0.43	0.42
	800	0.58	0.46	0.45	0.45	0.43	0.43
	750	0.57	0.46	0.45	0.44	0.43	0.42
	700	0.56	0.47	0.45	0.44	0.44	0.43
Vwind[c)]	Surface	0.62	0.48	0.44	0.43	0.43	0.42
	1000	0.61	0.46	0.45	0.45	0.44	0.43
	975	0.61	0.47	0.45	0.46	0.44	0.44
	950	0.59	0.48	0.46	0.45	0.44	0.43
	925	0.58	0.46	0.48	0.45	0.44	0.43
	900	0.57	0.48	0.45	0.44	0.44	0.43
	850	0.55	0.47	0.46	0.45	0.44	0.43
	800	0.54	0.48	0.46	0.45	0.44	0.43
	750	0.51	0.47	0.45	0.44	0.43	0.43
	700	0.48	0.46	0.46	0.44	0.44	0.43
PBLH[d)]	Surface	0.64	0.51	0.46	0.45	0.44	0.43

Notes: a) RH represented relative humidity; b) Uwind represented zonal wind; c) Vwind represented meridional wind; d) PBLH represented the height of planetary boundary layer.

important barrier to the transmission of aerosols in the eastern part of the study area. High-humidity air around the Bohai Sea and in the coastal areas to the east is conducive to the accumulation and development of pollutants, and thus has a greater impact on the pollution of the east side of the mountains. Due to the separation of mountains, the impact on the west side of the mountain range is less pronounced.

3.2.2 Wind & $PM_{2.5}$

Wind speed and wind direction highly affects $PM_{2.5}$ pollution level by diluting the concentration of pollutants or transferring particulate matters from different sources with varied properties to the study area (Adams et al., 2001; Jacob and Winner, 2009; Guo et al., 2014; Nguyen et al., 2017) and can frequently contribute to temporal variation in air pollutant concentrations further. Generally, wind speed has a certain impact on turbulence, affecting different dispersion conditions for pollutants or changing the nature of gas flow and the direction of pollutants' transportation (Tian et al., 2014; Zhou et al., 2015). Therefore, we analyzed the relationship between Uwind, Vwind and $PM_{2.5}$ respectively.

$PM_{2.5}$ concentrations over the south-eastern to northern part of North China was mainly negatively correlated with

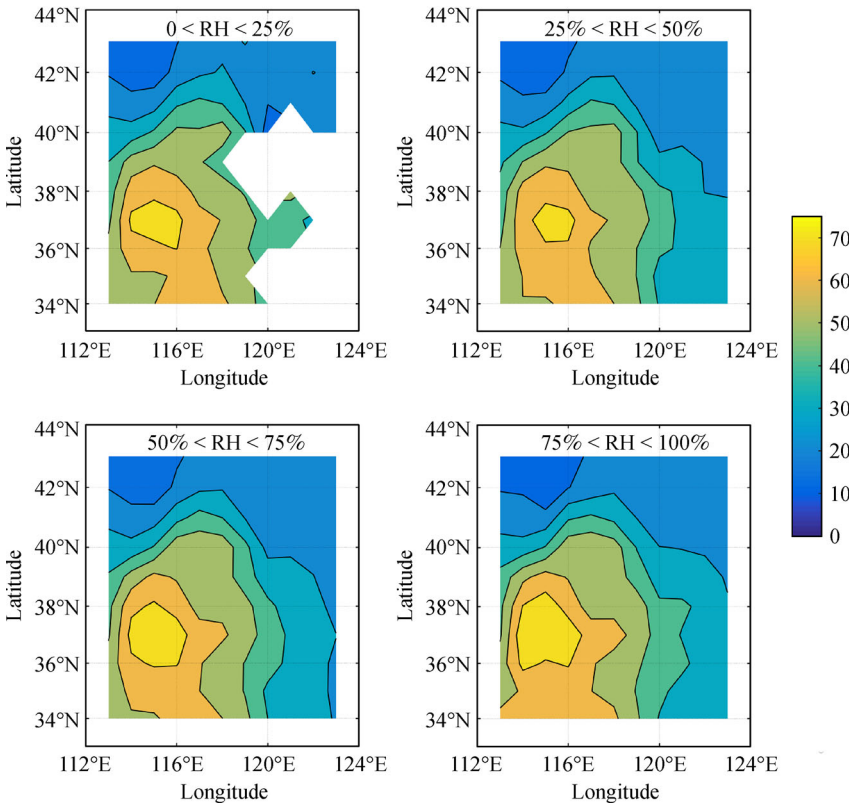

Fig. 5 Spatial distribution of the average $PM_{2.5}$ concentrations in different relative humidity intervals during study period, the unit for the color bar is μg/cm^3.

the zonal wind in north-western and south-eastern regions of North China (R = 0.6) (Fig. 7). This indicated that the greater the easterly wind speed in the south-eastern and north-western regions of North China (especially for the area close to the mountains), the heavier the pollution in the eastern part of the Taihang Mountains becomes – except for the Shandong Peninsula. Judging from the meridional wind V, south wind becomes a favorable meteorological condition for the accumulation of pollution compared to north wind. $PM_{2.5}$ concentration from the south-eastern to northern part of North China was mainly positively correlated with the meridian winds around the high $PM_{2.5}$ value center (R = 0.6). The greater the southerly winds around the high-pollution center, the pollution in the eastern part of the Taihang Mountains becomes heavier – except for the Shandong Peninsula.

There are three main explanations: different air characteristics carried by varied directional wind, industrial distribution and topographic changes from the south-east to the north-west. As mentioned before, North China is located in the transitional zone of the eastern coast and inland region in the west of China. Therefore, the wind blowing from the east and the south is mainly accompanied by warm and humid air, while air carried by the north and west winds are relatively dry and cold. What's more, industries are mainly distributed north of Henan, south of Hebei and east of Shandong Province; which means winds from southern and easterly directions will carry a lot of pollution particles. Considering the influence of relative humidity on $PM_{2.5}$ above, air that followed east and south winds (with large amounts of industrial emissions of particulates) was more conducive to the formation and accumulation of pollutants – especially when together with the blocking effect of the Taihang Mountains.

3.2.3 PBLH & $PM_{2.5}$

Similarly, as with RH, we divided PBLH into 5 intervals from less than 1000m to larger than 3000m. This is essential as the height of planetary boundary layer affects the behavior of pollutants in the atmosphere (Marcazzan et al., 2001; Liu et al., 2005; Sotoudeheian and Arhami, 2014). Displayed in Fig. 8, $PM_{2.5}$ pollution was most severe when the boundary layer height was between 1500 and 2500 m. From the point of view of atmospheric dynamics, the higher the planetary boundary layer, the more conducive to the diffusion of aerosol particles and also the meteorological conditions conducive to pollution dispersal. When the height of the boundary layer is very low, the weather system is prone to occur with precipitation mostly and similarly conducive to contamination settlement. Our results approved these regulars.

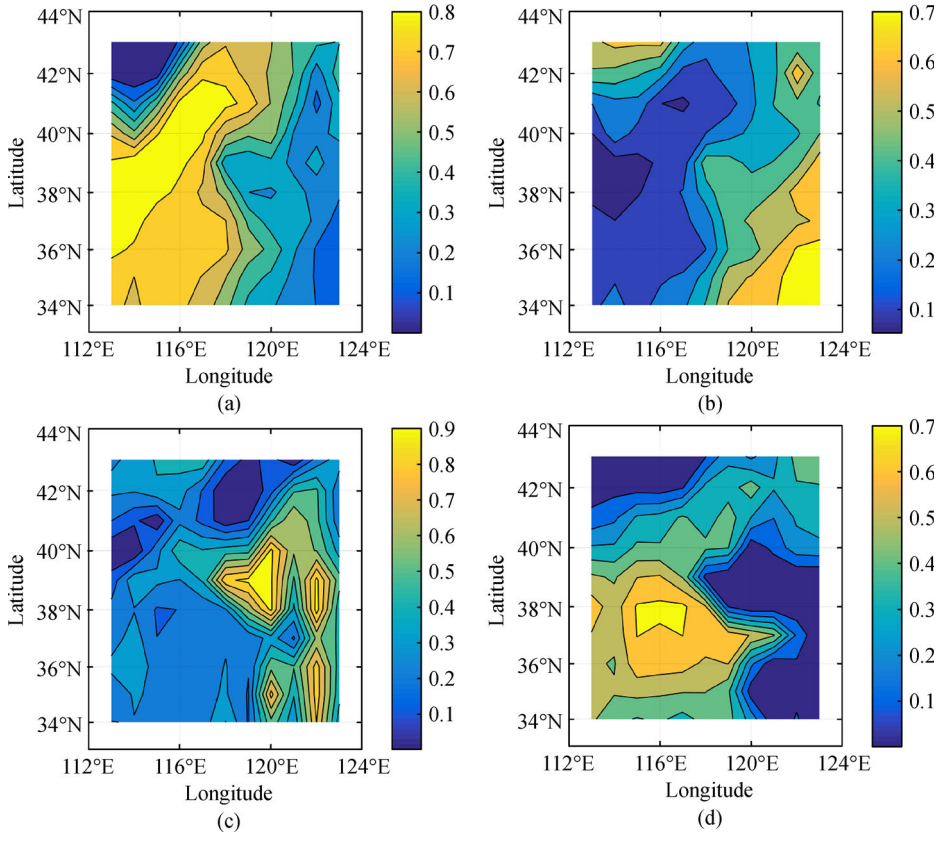

Fig. 6 Spatial distribution of the correlation coefficient of RH with its (a) first and second (b) typical variable and $PM_{2.5}$ with its (c) first and second (d) typical variable. Through these relationships and the correlation coefficient of each pair of typical variables, the correlation between the corresponding $PM_{2.5}$ and meteorological elements can be known.

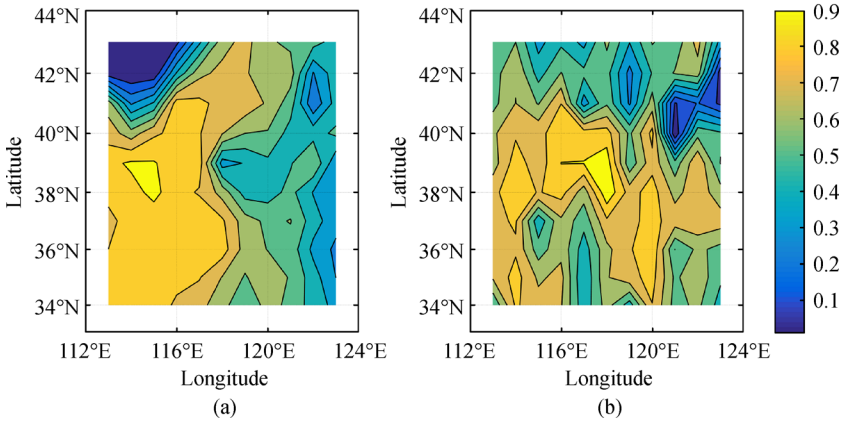

Fig. 7 Spatial distribution of the correlation coefficient of Uwind with its (a) first typical variable and (b) $PM_{2.5}$ with its first typical variable.

Seeing from CCA, $PM_{2.5}$ concentrations from the south-eastern to northern part of North China was mainly negatively correlated with the boundary layer height of the northern and south-eastern parts. Which means the lower the planetary boundary layer in the southern and northern part, the greater the pollution concentration in the pollution center.

From the above analysis, we can know that the first typical correlation factor between $PM_{2.5}$ and several meteorological elements all described the relationship between meteorological elements and the high value of $PM_{2.5}$ pollution in North China. This showed that the spatial distribution of $PM_{2.5}$ in North China was relatively fixed, and the overall discharge status of the region determines the $PM_{2.5}$ pollutions in an area, and that the meteorological conditions only affect the distribution of

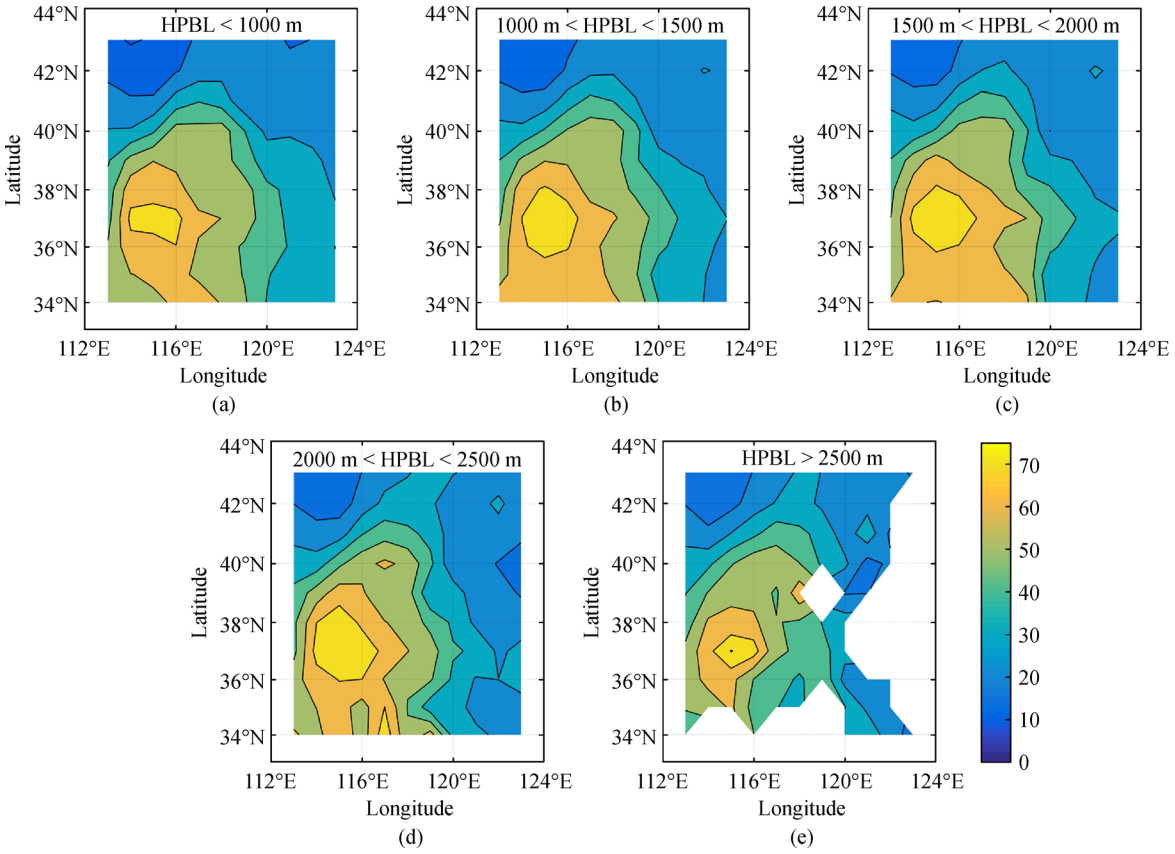

Fig. 8 Spatial distribution of the average $PM_{2.5}$ concentrations in different height of planetary boundary layer intervals during study period, the unit for the color bar is $\mu g/cm^3$.

short-term particulate matters.

Notably, when the wind speed exceeds a certain threshold, the south wind and the east wind may also carry favorable conditions for $PM_{2.5}$ proliferations. Generally, the south wind and east wind with wind speeds in the range of 0–5m/s easily lead to pollution formation according to studies by Zhou and Zhao (2017). Beside the parameters we mentioned before, other meteorological parameters like temperature, precipitation also affect $PM_{2.5}$ concentrations. For example, characterized by anticyclonic condition, weak wind, no precipitation, usually accompanied by high temperatures stagnation illustrates strong association with high $PM_{2.5}$ levels (Tai et al., 2010). We analyzed the effect of individual meteorological factors on the concentration of $PM_{2.5}$, but the meteorological factors are coupled to each other and cannot occur independently. Under the influence of other meteorological elements, the effect over the concentration of $PM_{2.5}$ may weaken and even change the influence direction. Therefore, it remains to be explored how to identify the factors that have the greatest influence on the concentration of $PM_{2.5}$ in a meteorological field and how the $PM_{2.5}$ concentration interacts with meteorological factors of different performances.

4 Conclusions

This study derived high-resolution daily ground-level $PM_{2.5}$ concentration data using 3 km MODIS AOD products with complete spatial coverage over North China between the 2003–2015 period. Mixed effect modeling was developed to simulate AOD-$PM_{2.5}$ relationships, while canonical correlation analysis was applied to analyze the impact of meteorological elements on $PM_{2.5}$. Through that, we captured the spatial distribution with one high-value and two low-value areas over the study area and temporal characteristics with low $PM_{2.5}$ pollution in 2004, 2009 and after 2013.

Satellite AOD data have been increasingly used in conjunction with in site $PM_{2.5}$ ground observations, due to its high spatial and temporal resolution – especially for North China where pollution is particularly high but ground observations start late and observation sites are sparse. Future satellite technologies will provide data with finer spatial and temporal resolutions and more accurate AOD retrieval data. What's more, multi-level AOD data in vertical space can also be observed and released now. With the help of these technologies, $PM_{2.5}$ concentration inverted by AOD in the future will be more accurate and

precise, which will help control and predict $PM_{2.5}$ concentrations.

This research mainly focused on the spatio-temporal changes of $PM_{2.5}$ pollutions in North China, but the impact on meteorological factors was only discussed initially. In the future, the coupling effect of meteorological elements on the impact of $PM_{2.5}$ must be further studied to provide more accurate information on $PM_{2.5}$ governance and forecasting.

Acknowledgements This study was funded by the National Key Technology R&D Program (Grant No. 2018YFA0606104) and the National Natural Science Foundation of China (Grant No. 41471073).

References

Adams H S, Nieuwenhuijsen M J, Colvile R N (2001). Determinants of fine particle ($PM_{2.5}$) personal exposure levels in transport micro-environments, London, UK. Atmospheric Environment, 35(27): 4557–4566

Bai Y, Wu L, Qin K, Zhang Y, Shen Y, Zhou Y (2016). A geographically and temporally weighted regression model for ground-level $PM_{2.5}$ estimation from satellite-derived 500 m resolution AOD. Remote Sensing, 8(3): 262–282

Beloconi A, Kamarianakis Y, Chrysoulakis N (2016). Estimating urban PM_{10} and $PM_{2.5}$ concentrations, based on synergistic meris/aatsr aerosol observations, land cover and morphology data. Remote Sensing of Environment, 172: 148–164

Cao G, Zhang X, Gong S, An X, Wang Y (2011). Emission inventories of primary particles and pollutant gases for China. Chinese Science Bulletin, 56(8): 781–788 (in Chinese)

Chen S, Guo J, Song L, Li J, Liu L, Cohen J B (2019). Inter-annual variation of the spring haze pollution over the North China Plain: Roles of atmospheric circulation and sea surface temperature. International Journal of Climatology, 39(2): 783–798

Chen Y, Zhao C S, Zhang Q, Deng Z Z, Huang M Y, Ma X C (2009). Aircraft study of mountain chimney effect of Beijing, China. Journal of Geophysical Research, 114, D08306DeGaetano AT, Doherty OM (2004). Temporal, spatial and meteorological variations in hourly $PM_{2.5}$ concentration extremes in New York City. Atmospheric Environment, 38: 1547–1558

Dinoi A, Perrone M R, Burlizzi P (2010). Application of MODIS Products for Air Quality Studies Over Southeastern Italy. Remote Sensing, 2(7): 1767–1796

Duan J, Tan T (2003). Atmospheric heavy metals and arsenic in China: Situation, sources and control policies. Atmospheric Environment, 74: 93–101

Engel-Cox J A, Hoff R M, Rogers R, Dimmick F, Rush A C, Szykman J J, Al-Saadi J, Chu D A, Zell E R (2006). Integrating lidar and satellite optical depth with ambient monitoring for 3-dimensional particulate characterization. Atmospheric Environment, 40(40): 8056–8067

Fan Y, Chun C (2008). Visibility trends in Beijing, Tianjin and Hebei Province during 1980–2003. Plateau Meteorology, 27: 1392–1400 (in Chinese)

Fang G C, Wu Y S, Wen C C, Lee W J, Chang S Y (2007). Influence of meteorological parameters on particulates and atmospheric pollutants at Taichung harbor sampling site. Environmental Monitoring and Assessment, 128(1-3): 259–275

Ghotbi S, Sotoudeheian S, Arhami M (2016). Estimating urban ground-level PM_{10} using MODIS 3 km AOD product and meteorological parameters from WRF model. Atmospheric Environment, 141: 333–346

Gu Y, Yim S H (2016). The air quality and health impacts of domestic trans-boundary pollution in various regions of China. Environment International, 97: 117–124

Guo J, Deng M, Lee S S, Wang F, Li Z, Zhai P, Liu H, Lv W, Yao W, Li X (2016). Delaying precipitation and lightning by air pollution over the Pearl River Delta. Part I: Observational analyses. Journal of Geophysical Research, D, Atmospheres, 121(11): 6472–6488

Guo J, Zhang X, Wu Y, Zhaxi Y, Che H, La B, Wang W, Li X (2011). Spatio-temporal variation trends of satellite-based aerosol optical depth in China during 1980–2008. Atmospheric Environment, 45 (37): 6802–6811

Guo Y, Feng N, Christopher S A, Kang P, Zhan F B, Hong S (2014). Satellite remote sensing of fine particulate matter ($PM_{2.5}$) air quality over Beijing using MODIS. International Journal of Remote Sensing, 35(17): 6522–6544

Gupta P, Christopher S A (2008). Seven year particulate matter air quality assessment from surface and satellite measurements. Atmospheric Chemistry and Physics, 8(12): 3311–3324

Henderson C R (1948). Estimation of general, specific and maternal combining abilities in crosses among inbred lines of swine. NIDA Research Monograph, 37: 241–270

Hotelling H (1936). Relations between two sets of variates. Biometrika, 28(3-4): 321–377

Hu X, Waller L A, Lyapustin A, Wang Y, Al-Hamdan M Z, Crosson W L, Estes M G Jr, Estes S M, Quattrochi D A, Puttaswamy S J, Liu Y (2014). Estimating ground-level $PM_{2.5}$ concentrations in the Southeastern United States using MAIAC AOD retrievals and a two-stage model. Remote Sensing of Environment, 140: 220–232

Hu Y, Zhou Z (2009). Climatic Characteristics of Haze in China. Meteorological Monographs, 35: 73–78 (in Chinese)

Jacob D J, Winner D A (2009). Effect of climate change on air quality. Atmospheric Environment, 43(1): 51–63

Jiang J H, Su H, Huang L, Wang Y, Massie S, Zhao B, Omar A, Wang Z (2018). Contrasting effects on deep convective clouds by different types of aerosols. Nature Communications, 9(1): 1–7

Kalnay E, Kanamitsu M, Kistler R, Collins W, Deaven D, Gandin L, Iredell M, Saha S, White G, Woollen J, Zhu Y, Chelliah M, Ebisuzaki W, Higgins W, Janowiak J, Mo K C, Ropelewski C, Wang J, Leetmaa A, Reynolds R, Jenne R, Joseph D (1996). The NCEP/NCAR 40-year reanalysis project. Bulletin of the American Meteorological Society, 77(3): 437–471

Kaufman Y J, Tanré D, Boucher O (2002). A satellite view of aerosols in the climate system. Nature, 419(6903): 215–223

Kloog I, Nordio F, Coull B A, Schwartz J (2012). Incorporating local land use regression and satellite aerosol optical depth in a hybrid model of spatiotemporal $PM_{2.5}$ exposures in the Mid-Atlantic states. Environmental Science & Technology, 46(21): 11913–11921

Koren I, Altaratz O, Remer A, Feingold G, Vanderlei J, Heiblum H (2012). Aerosol-induced intensification of rain from the tropics to the

mid-latitudes. Nature Geoscience, 5(2): 118–122

Lee H J, Chatfield R B, Strawa A W (2016). Enhancing the applicability of satellite remote sensing for $PM_{2.5}$ estimation using MODIS deep blue AOD and land use regression in California, United States. Environmental Science & Technology, 50(12): 6546–6555

Lee H J, Liu Y, Coull B A, Schwartz J, Koutrakis P (2011). A novel calibration approach of MODIS AOD data to predict $PM_{2.5}$ concentrations. Atmospheric Chemistry and Physics, 11(15): 7991–8002

Levy R C, Hsu C (2015). MODIS Atmosphere L2 Aerosol Product. NASA MODIS Adaptive Processing System, Goddard Space Flight Center, USA. Doi:10.5067/MODIS/MYD04_L2.061

Levy R C, Mattoo S, Munchak L A, Remer L A, Sayer A M, Patadia F, Hsu N C (2013). The Collection 6 MODIS aerosol products over land and ocean. Atmospheric Measurement Techniques, 6(11): 2989–3034

Levy R C, Remer L A, Kleidman R G, Mattoo S, Ichoku C, Kahn R, Eck T F (2010). Global evaluation of the Collection 5 MODIS dark-target aerosol products over land. Atmospheric Chemistry and Physics, 10 (21): 10399–10420

Li G, Fang C, Wang S, Sun S (2016). The effect of economic growth, urbanization, and industrialization on fine particulate matter ($PM_{2.5}$) concentrations in China. Environmental Science & Technology, 50 (21): 11452–11459

Liu Y, Franklin M, Kahn R, Koutrakis P (2007). Using aerosol optical thickness to predict ground-level $PM_{2.5}$ concentrations in the St. Louis area: A comparison between MISR and MODIS. Remote Sensing of Environment, 107(1-2): 33–44

Liu Y, Paciorek C J, Koutrakis P (2009). Estimating regional spatial and temporal variability of $PM_{2.5}$ concentrations using satellite data, meteorology, and land use information. Environmental Health Perspectives, 117(6): 886–892

Liu Y, Park R J, Jacob D J, Li Q, Kilaru V, Sarnat J A (2004). Mapping annual mean ground-level $PM_{2.5}$ concentrations using Multiangle Imaging Spectroradiometer aerosol optical thickness over the contiguous United States. Journal of Geophysical Research, D, Atmospheres, 109: D22206

Liu Y, Sarnat J A, Kilaru V, Jacob D J, Koutrakis P (2005). Estimating ground-level $PM_{2.5}$ in the eastern United States using satellite remote sensing. Environmental Science & Technology, 39(9): 3269–3278

Lorenz E N (1956). Emprical orthogonal functions and statistical weather prediction. Cambridge: Statistical Forecasting Project Department of Meteorology, MIT

Lv B, Hu Y, Chang H H, Russell A G, Cai J, Xu B, Bai Y (2017). Daily estimation of ground-level $PM_{2.5}$ concentrations at 4 km resolution over Beijing-Tianjin-Hebei by fusing MODIS AOD and ground observations. Science of the Total Environment, 580: 235–244

Ma Z, Hu X, Huang L, Bi J, Liu Y (2014). Estimating ground-level $PM_{2.5}$ in China using satellite remote sensing. Environmental Science & Technology, 48(13): 7436–7444

Ma Z, Liu Y, Zhao Q, Liu M, Zhou Y, Bi J (2016). Satellite-derived high resolution $PM_{2.5}$ concentrations in Yangtze River Delta Region of China using improved linear mixed effects model. Atmospheric Environment, 133: 156–164

Marcazzan G M, Vaccaro S, Valli G, Vecchi G (2001). Characterisation of PM_{10} and $PM_{2.5}$ particulate matter in the ambient air of Milan (Italy). Atmospheric Environment, 35(27): 4639–4650

Munchak L A, Levy R C, Mattoo S, Remer L A, Holben B N, Schafer J S, Hostetler C A, Ferrare R A (2013). MODIS 3 km aerosol product: applications over land in an urban/suburban region. Atmospheric Measurement Techniques, 6(7): 1747–1759

Nguyen M V, Park G H, Lee B K (2017). Correlation analysis of size-resolved airborne particulate matter with classified meteorological conditions. Meteorology and Atmospheric Physics, 129(1): 35–46

Pearce J L, Beringer J, Nicholls N, Hyndman R J, Uotila P, Tapper N J (2011). Investigating the influence of synoptic-scale meteorology on air quality using self-organizing maps and generalized additive modeling. Atmospheric Environment, 45(1): 128–136

Remer L A, Kaufman Y J, Tanré D, Mattoo S, Chu D A, Martins J V, Li R R, Ichoku C, Levy R C, Kleidman R G, Eck T F, Vermote E, Holben B N (2005). The MODIS Aerosol Algorithm, Products, and Validation. American Meteorological Society, 62(4): 947–973

Sotoudeheian S, Arhami M (2014). Estimating ground-level PM_{10} using satellite remote sensing and ground-based meteorological measurements over Tehran. Journal of Environmental Health Science & Engineering, 12(1): 122–134

Sun K, Chen X (2017). Spatio-temporal distribution of localized aerosol loading in China: A satellite view. Atmospheric Environment, 163: 35–43

Sun Y, Jiang Q, Wang Z, Fu P, Jie L, Yang T, Yin Y (2014). Investigation of the sources and evolution processes of severe haze pollution in Beijing in January 2013. Journal of Geophysical Research, D, Atmospheres, 119(7): 4380–4398

Tai A P K, Mickley L J, Jacob D J (2010). Correlations between fine particulate matter ($PM_{2.5}$) and meteorological variables in the United States: Implications for the sensitivity of $PM_{2.5}$ to climate change. Atmospheric Environment, 44(32): 3976–3984

Tian G, Qiao Z, Xu X (2014). Characteristics of particulate matter (PM_{10}) and its relationship with meteorological factors during 2001–2012 in Beijing. Environmental Pollution, 192: 266–274

Trenberth K E, Fasullo J T, Branstator G, Phillips A S (2014). Seasonal aspects of the recent pause in surface warming. Nature Climate Change, 4(10): 911–916

van Donkelaar A, Martin R V, Levy R C, da Silva A M, Krzyzanowski M, Chubarova N E, Semutnikova E, Cohen A J (2011). Satellite-based estimates of ground-level fine particulate matter during extreme events: A case study of the Moscow fires in 2010. Atmospheric Environment, 45(34): 6225–6232

Wang J, Christopher S A (2003). Intercomparison between satellite-derived aerosol optical thickness and $PM_{2.5}$ mass: Implications for air quality studies. Geophysical Research Letters, 30(21): 2095–2099

Wang L, Chen W (2014). A CMIP5 multimodel projection of future temperature, precipitation, and climatological drought in China. International Journal of Climatology, 34(6): 2059–2078

Wang Q, Huang R J, Zhao Z, Cao J, Ni H, Tie X, Zhao S, Su X, Han Y, Shen Z, Wang Y, Zhang N, Zhou Y, Corbin J C (2016). Physicochemical characteristics of black carbon aerosol and its radiative impact in a polluted urban area of China. Journal of Geophysical Research, D, Atmospheres, 121(20): 12505–12519

Wang Y, Wang H, Chang S, Liu M (2017). Higher-order network analysis of fine particulate matter ($PM_{2.5}$) transport in China at city level. Scientific Reports, 7(1): 13236–13244

Wei J, Jin Q, Yang Z L, Zhou L (2017). Land-atmosphere-aerosol coupling in North China during 2000–2013. International Journal of Climatology, 37: 1297–1306

Wu D, Wu X, Li F (2010). Temporal and spatial variation of haze during 1951–2005 in Chinese mainland. Acta Meteorologica Sinica, 68: 680–688 (in Chinese)

Xie Y, Wang Y, Zhang K, Dong W, Lv B, Bai Y (2015). Daily estimation of ground-level $PM_{2.5}$ concentrations over Beijing using 3 km resolution MODIS AOD. Environmental Science & Technology, 49(20): 12280–12288

Zhang Q, Jiang X, Tong D, Davis S J, Zhao H, Geng G, Feng T, Zheng B, Lu Z, Streets D G, Ni R, Brauer M, van Donkelaar A, Martin R V, Huo H, Liu Z, Pan D, Kan H, Yan Y, Lin J, He K, Guan D (2017a). Transboundary health impacts of transported global air pollution and international trade. Nature, 543(7647): 705–709

Zhang Q, Streets D G, Carmichael G R, He K B, Huo H, Kannari A, Klimont Z, Park I S, Reddy S, Fu J S, Chen D, Duan L, Lei Y, Wang L T, Yao Z L (2009). Asian emissions in 2006 for the NASA INTEX-B mission. Atmospheric Chemistry and Physics, 9(14): 5131–5153

Zhang R, Jing J, Tao J, Hsu S C, Wang G, Cao J, Lee C S L, Zhu L, Chen Z, Zhao Y, Shen Z (2013). Chemical characterization and source apportionment of $PM_{2.5}$ in Beijing: Seasonal perspective. Atmospheric Chemistry and Physics, 13(14): 7053–7074

Zhang R, Wang G, Guo S, Zamora M L, Ying Q, Lin Y, Wang W, Hu M, Wang Y (2015). Formation of urban fine particulate matter. Chemical Reviews, 115(10): 3803–3855

Zhang Y L, Cao F (2015). Fine particulate matter ($PM_{2.5}$) in China at a city level. Scientific Reports, 5(1): 14884–14895

Zhang Z, Wu W, Wei J, Song Y, Yan X, Zhu L, Wang Q (2017b). Aerosol optical depth retrieval from visibility in China during 1973–2014. Atmospheric Environment, 171: 38–48

Zhao T, Ailiku, Feng J (2004). An intercomparison between NCEP reanalysis and observed data over China. Climatic and Environmental Research, 9: 278–294 (in Chinese)

Zheng Y, Xue T, Zhang Q, Geng G, Tong D, Li X, He K (2017). Air quality improvements and health benefits from China's clean air action since 2013. Environmental Research Letters, 12(11): 114020

Zhou W, Tie X, Zhou G, Liang P (2015). Possible effects of climate change of wind on aerosol variation during winter in Shanghai, China. Particuology, 20: 80–88 (in Chinese)

Zhou Y, Zhao X (2017). Correlation Analysis between $PM_{2.5}$ Concentration and Meteorological Factors in Beijing Area. Acta Scientiarum Naturalium Universitatis Pekinensis, 53: 111–124 (in Chinese)